Z. Phys. B - Condensed Matter 88, 321-326 (1992)

Condensed Matter
Zeitschrift für Physik B

Atomic-scale contrast mechanism in atomic force microscopy

H. Heinzelmann*, E. Meyer, D. Brodbeck, G. Overney, and H.-J. Güntherodt

Institut für Physik, Klingelbergstrasse 82, CH-4056 Basel, Switzerland

Received July 15, 1991; revised version March 24, 1992

Despite the early success of atomic force microscopy in imaging atomic structures on layered materials, much of the hope and expectation for the high resolution capability of this method have been subverted by puzzling experimental results and a poor understanding of the basic contrast mechanism. The fact that very high repulsive forces can be applied between the tip and the sample without losing atomic resolution has led to several different explanations of the imaging process. These include multiple tip-sample contact imaging, large elastic deformations of the sample, and friction-dominated image formation. Until very recently it was only possible to atomically resolve materials having layered structures, such as HOPG, BN, $MnPS_3$, mica, TaS_2 and $TaSe_2$. Here, we compare those images with the ones collected from surfaces of the predominantly ionic crystals LiF and PbS. Based on the comparison of these two classes of imaged materials, contrast mechanisms are discussed.

I. Introduction

With the atomic force microscope (AFM) [1] a new method has been introduced to look at the structure of solid surfaces as well as to study minute forces on a subnanometer scale. Additionally, AFM on a nanometer scale has given valuable information about technologically interesting insulating samples (for a recent review on force microscopy see [2]). Imaging with the AFM has been performed with attractive as well as repulsive forces, but highest spatial resolution is only possible in the regime of strong repulsive (contact) forces. In this regime atomic resolution on layered materials has ben readily obtained [3].

Despite this early success AFM still suffers from a lack of understanding of the basic contrast mechanism. In particular, studies of layered materials such as highly oriented pyrolitic graphite (HOPG) at atomic resolution have yielded a variety of puzzling observations. It is possible to image these surfaces with loading forces (i.e., repulsive forces between tip and sample) of up to 10^{-6} N without losing atomic resolution. These conditions are too extreme for a single atom tip in contact with the surface to be stable, and it is likely that a single atom would puncture the topmost graphite layer. Together with the fact that single atom defects have not been observed so far by AFM, this leads to the conclusion that the contact area is likely to be much larger than a typical single atomic dimension.

Researchers have invoked several explanations to account for these observations. These include tips interacting with the sample at numerous contacts ('multiple tips'), microflakes of sample material being dragged across the surface, the shearing of layers of sample material and a large elastic response of the sample and/or a mediating surface layer.

The demonstration of atomic resolution on harder, non-layered crystals represents an important step since it overcomes the problems of elastic response of layered materials. Individual atoms of ionic crystal surfaces, such as LiF [4], NaCl [5] and PbS have now been resolved with AFM. In formulating an imaging mechanism for these ionic materials, previous explanations valid only for layered samples can be excluded.

In this paper we summarize some of the high resolution AFM work performed in our laboratory. From atomic scale images of the layered compounds HOPG, $MnPS_3$, MoS_2 and $TaSe_2$, the effects of friction and multiple contact points are reviewed, and the contribution of a *lateral, frictional* force to the observed signal is identified as a major source of image contrast on layered materials. We then present atomically resolved images of the nonlayered ionic crystals LiF and PbS. These data are compared to Helium scattering data, and are discussed in the light of recent theoretical efforts. A monoatomic tip - model is in reasonable agreement with the experimental data, pointing to a different contrast mechanism for the two classes of materials discussed here.

* *Present address:* IBM Almaden Research Laboratory, 650 Harry Road, San Jose, CA 95120, USA

II. Experimental procedure

We use electron tunneling to measure the deflection of the probing cantilever. It is our experience that this method takes advantage of the superior sensitivity of the tunneling current and is very reliable as long as there is a good tunneling signal. Before each experiment, we freshly evaporate a gold layer on the lever backside. PtIr tunneling tips work more reliable than tungsten tips since they are more inert. We find these experimental details to be critical for the operation of the AFM. These conditions can be maintained over several days without needing to change either cantilever or tunneling tip.

As force probes we use SiO_2 cantilevers which are kindly provided by the Institut de Microtechnique at the Université de Neuchâtel. Force constants are between 0.1 and 0.7 N/m, standard values for this type of AFM experiments. Often no additional tip is attached to the cantilever; the micro-roughness of the SiO_2 is sufficient for atomic-scale imaging of flat surfaces, and nearly every cantilever gives atomic resolution.

The instrument is described in detail in previous publications [2, 6]. The key feature is an eccentric mechanism which allows a pure mechanical approach of sample and probe in steps as small as 50 Å. The microscope is operated on an antivibration table at scan rates between 20 and 80 Hz. Pictures are taken in the variable deflection mode, with both constant tunneling current and variable tunneling current conditions. We operate the instrument in the regime of repulsive contact forces in a nearly constant force mode. By performing force vs. distance curves adhesive forces and repulsive forces in the contact zone are determined. For the repulsive forces typical values of 10^{-8} N are found.

The samples with layered structures were mounted on sample holders and freshly cleaved with adhesive tape before being transferred to the microscope. As it is the case for HOPG and mica, also $MnPS_3$, MoS_2 and $TaSe_2$ all provide large flat areas upon cleavage, ideally suited for fast scan imaging. The non-layered samples are cleaved with a knife edge to expose a (001) surface. All the experiments described here are conducted at ambient conditions.

III. Friction-dominated imaging of layered materials

Soon after the first demonstration of atomic resolution on HOPG by AFM [3], several other layered compounds were imaged, such as highly oriented pyrolitic boron nitride [7] and $TaSe_2$ [8]. Since then atomic-scale resolution of layered materials by AFM has become standard. The interpretation of the data, however, is difficult, and many unresolved questions remain. In this chapter we will demonstrate that frictional forces are a very important contrast source for AFM of layered materials.

Figure 1 shows AFM images of HOPG. This surface consists of a hexagonal net of two inequivalent carbon atoms in a sense that every other carbon atom sits directly above a carbon atom in the layer beneath (*A* sites); the alternating atoms sit above the centers of the rings in the layer below (*B* sites). Figure 1a shows a hexagonal structure, every second corner appearing brighter than its neighbor. The observed periodicity corresponds to the known lattice spacing of 2.46 Å, within the experimental uncertainty of ± 0.1 Å. This pattern seems to reflect the atomic arrangement and the inequivalency of the atomic sites. A measurable difference in the force experienced by a tip over an *A* site and over a *B* site is, however, not predicted by calculations [9]. The experimental corrugation height is 0.1 to 0.3 Å, a value which is also found by other researchers [10] and compares well to Helium scattering data [11].

More often however an AFM image of HOPG only shows every second atom, as in Fig. 1b. The protrusions are spaced 2.5 ± 0.1 Å. These changes in the appearance of images of HOPG can be explained by changes in the relative amplitudes and phases of three dominant Fourier components [12], and can thus be caused by changes in the tip-sample contact.

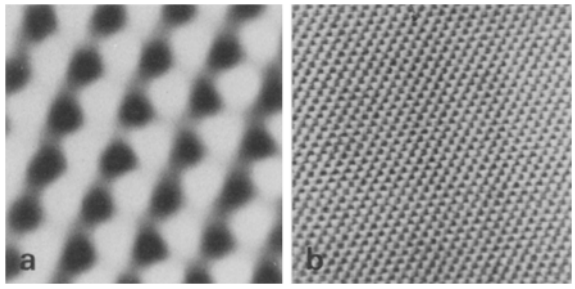

Fig. 1a, b. AFM images of HOPG. **a** showing a hexagonal net with 2 alternating inequivalent sites. **b** larger area, showing every other atom only

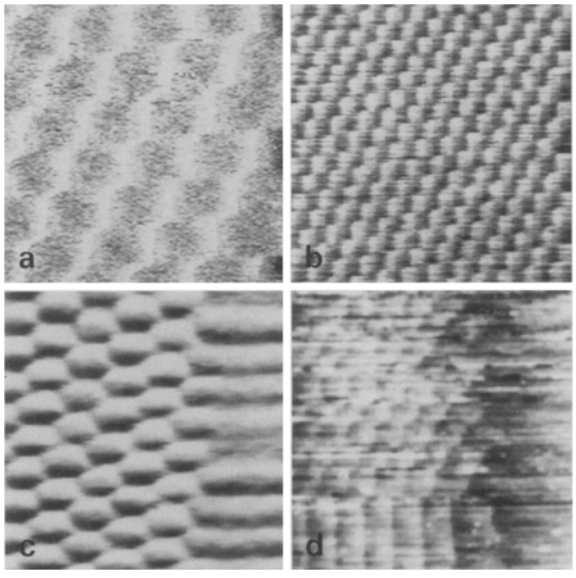

Fig. 2a–d. AFM images on layered materials showing strong distortions. **a** double tip imaging of HOPG. **b** tracking of the tip in the atomic lattice of a HOPG surface. **c** sticking to the lever at the beginning of each scan line on $MnPS_3$. **d** sticking of the lever to the sample in both scanning directions on 1 *T*-TaS_2

Image distortions become more pronounced at higher loading forces where the contact area is increased and multiple atom tip imaging and/or a stickslip behavior of the tip on the surface is more likely. Figure 2a shows the graphite lattice appearing as zig zag lines (one of the three dominant Fourier components is suppressed in this case). In Fig. 2b carbon atoms on HOPG appear as squares. This appearance is due to tip atoms tracking in the grooves of the surface lattice: the lever continues sliding between the same rows of atoms until the lateral tracking force induced by the scanning process exceeds a certain value. Then the tip jumps into the next row of atoms, and so forth, leading to an effective stick and slip behavior. Figure 2c shows a similar effect common to AFM images. It shows sulfur atoms on the surface of $MnPS_3$, a transparent insulator. The beginning of each scan line is heavily distorted (the image has been scanned from right to left). This is again due to friction: the lever initially sticks to the surface until a lateral force (imposed by the scanning process) is exerted which is large enough to overcome the static frictional force. This occurs at a point where the force gradient equals the lateral force constant of the cantilever. The distortion is obviously connected to the atomic positions, reflecting the variation of the frictional force on the atomic scale [13]. Finally, Fig. 2d shows the same type of distortion, but this time it occurs both at the beginning of each scanline and at the beginning of the whole frame (the area is scanned from the bottom to the top). The lattice constant deferred from this particular image is much too high, which also points to large frictional distortions.

To study those effects in more detail, we explored the dependence of the distortion on the applied loading force. Figure 3a shows an image of MoS_2 acquired with a loading force of 10^{-8} N, showing a layer of S atoms spaced 3.5 Å. Note the small distorted margin at the right edge. By increasing the force to 10^{-7} N the image changed dramatically (Fig. 3b), and an extreme stick-slip behavior of the tip can be seen. This is recognized more clearly in the asymmetric profile of a single scan line (Fig. 3d). The line shows a contour of constant force, the corrugation is increased to 5.0 Å as opposed to 1.5 Å for the image shown in Fig. 3a.

These corrugations do not agree with the ideal picture of an AFM tip tracing contours of constant charge density [3], which would lead to typical corrugations of some tenths of an Å. Furthermore, an idealized monoatomic tip is expected to puncture it [9]. However, these findings can be explained by assuming friction as the main contributor to the observed contrast. By increasing the load the contact area is increased, and therefore the frictional force between tip and sample is enhanced. Due to the tilt of the lever towards the sample as shown in Fig. 3c the frictional force corrugation ΔF_x contributes to the measured signal as $\Delta F_x = \Delta z \cdot c_B / \sin\alpha$. With a lever constant $c_B = 0.7$ /m, $\alpha \sim 20°$, and a loading of 10^{-7} (as in Fig. 3b), a frictional force ΔF_x of as little as 10^{-9} N is enough to cause a signal corrugation of 4.9 Å. Assuming that an extrapolation of the values reported by Mate et al. [13] down to loadings of 10^{-7} N is valid, a frictional force of 10^{-9} N is reasonable. The observed corrugation in Fig. 3b is 5.0 Å, so we conclude that this image is completely dominated by a frictional contrast mechanism.

This effect is believed to be of outermost importance for the imaging of charge density waves (CDW) by AFM. A CDW is a superstructure formed by a periodic lattice distortion of the atom cores accompanied by the charge modulation of the conduction electrons. In the case of 1 T-$TaSe_2$ a $\sqrt{13} \times \sqrt{13}$ superstructure is formed at room temperature. Helium scattering shows that the CDW propagates up to the sample surface. The corrugation of the CDW was determined to be 0.37 Å, the atomic corrugation was 0.52 Å [14, 15].

Figure 4a shows an AFM image of 1 T-$TaSe_2$. It is dominated by the atomic structure, whereas the CDW only contributes a small modulation of the signal. The

Fig. 3a–d. AFM images of MoS_2, with a frictional distortion at the beginning of each scan line. **a** image taken with an applied loading of 10^{-8} N; the corrugation is 1.5 Å. **b** image taken with an applied loading of 10^{-7} N, the corrugation is 5.0 Å. **c** illustration of cantilever-sample geometry during an experiment. **d** single scanline of **b**. The asymmetrical profile of the scanline is related to the influence of frictional forces

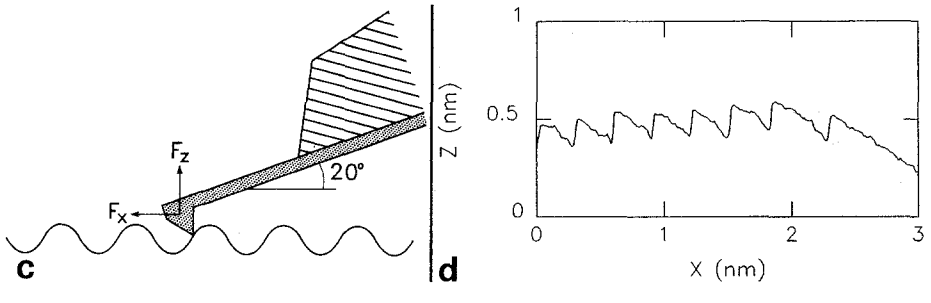

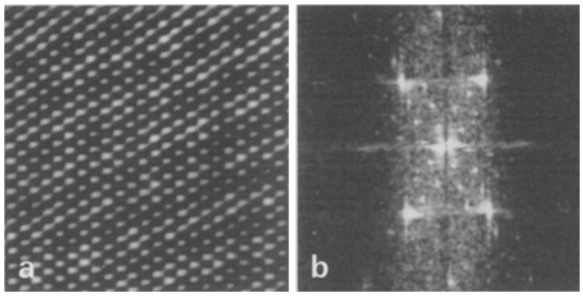

Fig. 4. AFM image of 1 T-$TaSe_2$, showing its charge density wave state **a** imaged with a force of 10^{-8} N; both the atomic and the superstructure are visible. **b** Corresponding Fourier transformed image. The inner peaks correspond to the $\sqrt{13}\times\sqrt{13}$ superstructure

superstructure can however be clearly observed in the two dimensional Fourier transformation (Fig. 4b). The periodicity of 11 ± 2 Å and the orientation of $15\pm2°$ relative to the atomic lattice are in good agreement with the expected values of 12.54 Å and 13.9°. Typical corrugation heights of the atomic lattice are between $0.5-2$ Å whereas the corrugation of the CDW is limited to ≈0.2 Å. Detailed examination of individual scanlines confirmed the pronounced presence of frictional distortion. In their first demonstration of AFM on CDWs Barret et al. speculated that it is this apparent frictional effect which allowed them to resolve the CDW corrugation [16]. The atomic corrugation, although distorted, shows only little noise and allows the resolution of the small additional CDW modulation. Although no definitive interpretation can be given at this point, it seems probable that the AFM responds to the periodic lattice distortion rather than to the charge modulation at the Fermi energy.

Summarizing the results on layered materials, atomic resolution is readily obtained, although the contrast mechanism is far from completely understood. The huge normal forces applied while still getting atomic resolution makes multiple contact points probable, otherwise tip and/or sample would not be stable [9, 17]. The observed corrugation heights are too large to be explained by a single tip atom above a rigid surface. They can, however be understood if we take frictional forces into account. Higher loadings lead to larger contact areas, increasing the tribological effect and thus the observed corrugation amplitudes. To directly measure the influence of frictional effects on an AFM image is generally difficult and requires an instrument which is able to monitor both normal and lateral force components of the lever deflection separately [18].

IV. Images of non-layered materials

In order to distinguish between the different possibilities for the contrast mechanism, we have applied AFM to another class of materials, ionic crystals. We have investigated LiF and PbS, both having a rocksalt crystal structure. They are thus isotropic, in contrast to the layered

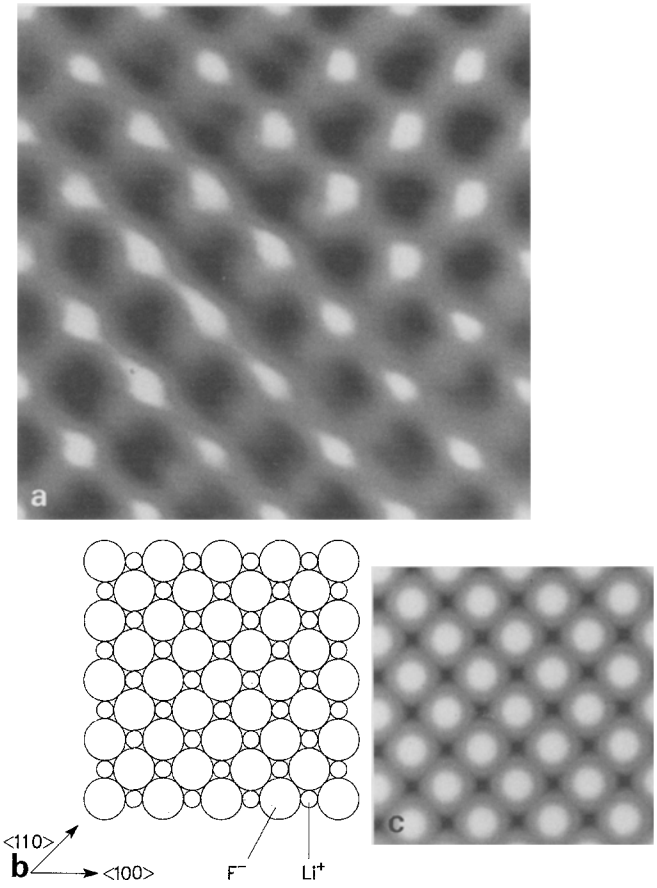

Fig. 5a–c. AFM on LiF (001). **a** experiment, showing protrusions 2.8 ± 0.1 Å apart; **b** model of the (001) surface of LiF, ions are shown as circle with their respective atomic radii; **c** contact hard sphere simulation, assuming one oxygen atom at the tip apex

materials, and are much harder and less likely to deform under the load of the AFM tip.

The (001) surface of LiF proves to be an ideal AFM sample [4]. It is reasonably inert in ambient atmosphere and is well characterized by Helium scattering experiments. LiF has a nearly pure ionic bonding character with a lattice constant of 4.02 Å. Figure 5a shows an atomically resolved image of LiF(001). The protrusions are regularly arranged in a square network and are spaced 2.8 ± 0.1 Å. This correspond to the distance between ions of the same sign, either Li^+ or F^-. A model of the surface is given in Fig. 5b, where the size of the ions represents their actual ionic radius, namely 0.68 Å for Li^+ and 1.33 Å for F^- [19].

The experimental corrugation height is 0.5 ± 0.1 Å in the $\langle100\rangle$ direction and 0.3 ± 0.1 Å in the $\langle110\rangle$ direction. These numbers are similar to the values found by Helium scattering experiments [20, 21], 0.61 Å in the $\langle100\rangle$ direction and 0.34 Å in the $\langle110\rangle$ direction.

In Helium scattering the situation can be described by the contact hard sphere model, also known as the corrugated hard wall model [21]. It can be concluded from this simple picture that the maxima seen in Helium scattering are attributable to the larger F^- ions. This simple model, however, does not account for details in the re-

pulsive part of the He-LiF interaction potential, which it simply assumes that the slope of the repulsive forces is indefinitely large.

With a loading force of 10^{-8} N we operate the AFM in the repulsive part of the interaction potential, so it is very likely that the AFM maxima correspond to fluorine ions. Figure 5c shows a simulated AFM scan, based on the hard sphere model and assuming an oxygen atom at the apex of the SiO_2 tip (radius 1.5 Å). The corrugation heights are 0.1 to 0.2 Å larger than those found in the AFM experiment, and the protrusions appear much too large. Recent calculations for a spherical diamond tip of radius 2 Å above the Li site of a (001) LiF surface suggest a tip sample distance of 3.48 Å for a repulsive force of 4.4×10^{-8} N [22]. This distance is much larger than $r(O^-)+r(Li^+)=2.18$ Å, assumed in the contact hard sphere model. This suggests that the AFM tip probes the surface at a point too low on the repulsive part of the interaction potential curve to be validly compared to Helium scattering. Unfortunately, no corresponding values for the F site nor constant force contours were given, so that we can not compare the corrugation heights with our experiment. While a detailed understanding of the contrast mechanism needs further investigation, the overall agreement of Helium scattering and AFM corrugations points to a monoatomic tip-sample interaction. This situation may be achieved by a mediating surface layer of water or ambient organics, and a microasperity of the tip effectively probing the sample surface.

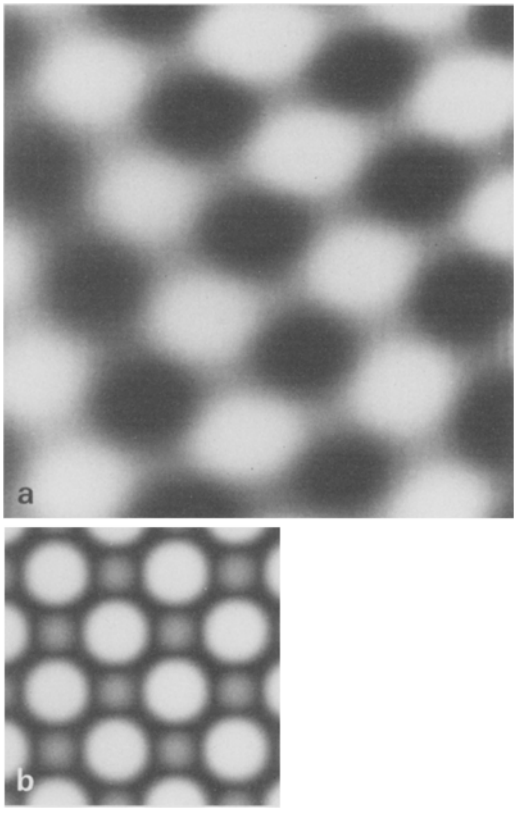

Fig. 6a, b. AFM on PbS (001). **a** experiment, showing protrusions 4.0 ± 0.2 Å apart; **b** contact hard sphere simulation, assuming one oxygen atom at the tip apex

Another sample resolved by AFM was PbS, a low bandgap semiconductor with a rocksalt structure with a lattice constant of 5.94 Å (Fig. 6a). The bonding character is ionic with a strong covalent contribution. The corrugation heights are comparable to our results on LiF.

The observed lattice spacing of 4.0 ± 0.2 Å again corresponds to the distance between the same kind of surface atoms. This fact is interesting to compare with STM experiments on PbS [23] where both atomic species have been visualized. At the present stage it is not possible to tell which surface site is imaged by AFM. The contact hard sphere model is shown as a scan simulation in Fig. 6b. The model is less likely to describe the situation adequately because of the strong covalent bonding character in PbS, which results in additional charge between the nuclei. With ionic radii of 1.20 Å for Pb^{2+} and 1.84 Å for S^{2-}, it suggests that the sulfur is imaged. An additional downwards relaxation of the sulfur ions is suggested by calculations [24]. This would slightly decrease the apparent size of the sulfur and make the lead ions visible, what is clearly not the case in our experiment.

It should be pointed out that the interpretation of AFM data on the basis of the contact hard sphere model is highly speculative. It neglects several important mechanisms. Ab initio Hartree Fock calculations for a SiO tip above a (001) MgO surface have predicted opposite contrasts, arising from whether Si or O is the front tip atom [25]. Further, although the elastic deformation of the sample under the load of tip is not as large as for the layered materials [25], this effect may not be neglected.

Summarizing, the AFM corrugations obtained on nonlayered materials indicate a single atom-surface interaction, although a quantitative description from models or even an unambiguous identification of different atomic sites on the surface is not clear. The atomic structure of the tip is probably not in registry with the sample surface structure and therefore the mechanism of constructive superposition of tip and sample structures is no longer viable to explain atomic resolution. From the low corrugation heights, comparable to those from helium scattering experiments, we conclude that frictional forces appear to play a minor role. This is consistent with a smaller elastic deformation of the surface which would not allow a larger contact area and an increase in frictional force. Imaging by a microasperity through a mediating surface layer, thus allowing tip stability along with high corrugation heights, may be a valid explanation.

V. Conclusions

Atomic resolution images on layered materials are readily obtained, but many questions about the contrast mechanism remain unanswered. Atomic resolution is possible with very high loading forces where frictional effects and multiple tip effects readily occur. Thus care has to be taken when interpreting AFM images, and experiments should be repeated with different tips and different loading forces. It is probable that large elastic deformations

of the sample and/or the possibility of dragging a microflake across the surface render this class of materials amenable to AFM since a larger contact area leads to an increased contribution of the frictional force to the observed signal.

Non-layered materials prove to be more difficult to resolve, probably as a consequence of their isotropic structure and smaller deformability. On the surfaces of LiF and PbS, both possess a rocksalt crystal structure, only one atomic species could be visualized, the other constituent of the surface not being visible. Whereas it is very likely that on LiF it is the F^- ion which is imaged, the situation is not so clear-cut for PbS. The corrugation heights seen in AFM point to a single-atom-tip-sample interaction and favor a model where the loading force is mediated by a surface layer of water or ambient organic contaminations. The surface would then be probed by a microasperity of the tip poking through this layer. Except for a distorted margin at the beginning of each scan line which is due to a sticking of the lever to the sample surface, other image distortions occur more seldom.

The contrast mechanism on ionic crystals appears to be fundamentally different from the one encountered on layered materials. For further investigations, a better characterization of the tip is needed in terms of arrangement and chemical nature of the front atoms. A theoretical description of the corrugation height on deformable surfaces would help to understand the influence of local sample elasticity on the contrast mechanism.

It is a pleasure to acknowledge J. Frommer for helpful discussions, R. Buser and N. deRooij from the Institut de Microtechnique of Neuchâtel for kindly providing the microfabricated cantilevers used in these experiments, and F. Lévy and H. Berger for providing the $MnPS_3$, MoS_2 and TaS_2 samples. This work was financially supported by the Swiss National Science Foundation and the Kommission zur Förderung der wissenschaftlichen Forschung.

References

1. Binnig, G., Quate, C.F., Gerber, Ch.: Phys. Rev. Lett. **56**, 930 (1986)
2. Heinzelmann, H., Meyer, E., Rudin, H., Güntherodt, H.-J.: In: Proceedings of the NATO Meeting. Basic Concepts and Applications of Scanning Tunneling Microscopy (STM) and Related Techniques, held in Erice, April 17–29, 1989. London, New York: Kluwer Academic Publishers 1990
3. Binnig, G., Gerber, Ch., Stoll, E., Albrecht, T.R., Quate, C.F.: Europhys. Lett. **3**, 1281 (1987)
4. Meyer, E., Heinzelmann, H., Rudin, H., Güntherodt, H.-J.: Z. Phys. B – Condensed Matter **79**, 3 (1990)
5. Meyer, G., Amer, N.: App. Phys. Lett. **56**, 2100 (1990)
6. Meyer, E., Heinzelmann, H., Grütter, P., Jung, Th., Weisskopf, Th., Hidber, H.-R., Lapka, R., Rudin, H., Güntherodt, H.-J.: J. Microsc. **151**, 269 (1988)
7. Albrecht, T.R., Quate, C.F.: J. Appl. Phys. **62**, 2599 (1987)
8. Meyer, E., Anselmetti, D., Wiesendanger, R., Güntherodt, H.-J., Lévy, F., Berger, H.: Europhys. Lett. **9**, 695 (1989)
9. Abraham, F.F., Batra, I.P.: Surf. Sci. **209**, L125 (1989)
10. Albrecht, T.R., Quate, C.F.: J. Vac. Sci. Technol. A**6**, 271 (1988)
11. Boato, G., Cantini, P., Tatarek, R.: Phys. Rev. Lett. **40**, 887 (1979)
12. Mizes, H.A., Sang Jl Park, Harrison, W.A.: Phys. Rev. B**36**, 4491 (1987)
13. Mate, C.M., McClelland, G.M., Erlandsson, R., Chiang, S.: Phys. Rev. Lett. **59**, 1942 (1987)
14. Boato, G., Cantini, P., Colella, R.: Phys. Rev. Lett. **42**, 1635 (1979)
15. Cantini, P., Boato, G., Colella, R.: Physica B**99**, 59 (1980)
16. Barrett, R.C., Nogami, J., Quate, C.F.: App. Phys. Lett. **57**, 992 (1990)
17. Overney, G., Zhong, W., Tománek, D.: J. Vac. Sci. Tech. B**9**, 479 (1991)
18. Neubauer, G., Cohen, S.R., McClelland, G.M., Horne, D., Mate, C.M.: Rev. Sci. Instrum. **61**, 2296 (1990)
19. Kittel, C.: Introduction to solid state physics, 4th edn. New York: Wiley 1971
20. Boato, G., Cantini, P., Mattera, L.: Surf. Sci. **55**, 141 (1976)
21. Garciá, N.: J. Chem. Phys. **67**, 897 (1977)
22. Labeke, D. van, Labani, B., Girard, C.: Chem. Phys. Lett. **162**, 399 (1989)
23. Wilson, I.H., Zheng, N.J., Knipping, U., Tsong, S.T.: Appl. Phys. Lett. **53**, 2039 (1988)
24. de Wette, F.W., Kress, W., Schröder, U.: Phys. Rev. B**32**, 4143 (1985)
25. Shluger, A., Pisani, C., Roetti, C., Orlando, R.: J. Vac. Sci. Technol. A**8**, 3967 (1990)